Cement and Concrete Composites 163 (2025) 106212

Contents lists available at ScienceDirect

Cement and Concrete Composites

journal homepage: www.elsevier.com/locate/cemconcomp

Sensitivity of the test conditions for direct assessment of dynamic shear properties of fibre-reinforced cementitious composites (FRCC) with Split-Hopkinson bar

Cesare Signorini [a,*], Ahmed Tawfik [a], Daniele Forni [b], Viktor Mechtcherine [a], Ezio Cadoni [b]

[a] Institute of Construction Materials, TUD Dresden University of Technology, 01062 Dresden, Germany
[b] University of Applied Sciences and Arts of Southern Switzerland – DynaMat SUPSI Laboratory, Mendrisio, 6850, Switzerland

ARTICLE INFO

Keywords:
Dynamic shear
Fibre-reinforced concrete
Punching-through-shear
Split-Hopkinson bar

ABSTRACT

Fibre-reinforced cement-based composites (FRCCs) possess pronounced toughness due to the crack-bridging effect of the fibres and represent effective solutions for protecting concrete members against extreme events. In the scenario of localised impacts, protective FRCC overlays are subjected to severe punching shear, for which careful design is required. However, the dynamic shear characterisation of FRCC is complex due to the interplay of different phases in the composite (i.e. cementitious matrix, fibres, and their interaction), and standardised test methods for dynamic shear have yet to be developed. This paper focuses on the dynamic shear characterisation of a high-toughness FRCC based on a fine-grained cementitious matrix containing synthetic fibres. The emphasis is on the sensitivity of the material properties to three different test methods based on the Split-Hopkinson bar approach. Two Split-Hopkinson Tension Bar (SHTB) systems with different load wave generation principles (i.e. gravity versus pretensioned bar) and the same shear adapter for applying pure shear loading are considered. A third setup based on a Split Hopkinson Pressure Bar (SHPB) with coaxial specimens and a punch-through-shear configuration is considered as a benchmark. The results show that, when the same strain rate is applied, the confinement of the sample plays the key role in the determination of the shear properties of FRCCs, while different wave forms coming from different loading schemes are less influential. The sensitivity of the material response as a function of the specimen boundary condition emerged from this study highlights the need for consistent test protocols tailored on the intended application.

1. Introduction

Existing reinforced concrete (RC) structures are vulnerable to highly dynamic and extreme loading scenarios due to explosions, earthquakes, collisions, and warfare. The development and implementation of appropriate strengthening techniques is therefore urgently advocated to withstand the severe stresses generated by dynamic loading and to protect structures and infrastructure. For such critical applications, mineral-bonded fibre reinforced composites with high strength, ductility and energy absorption capability are required and a thorough and accurate characterisation at high strain rates is necessary for design purposes. The most popular technique for studying the high strain rate behaviour of materials and composites is the Kolsky bar [1], widely known as the Split-Hopkinson bar (SHB), which examines a strain rate domain between 10^2 and 10^4 s^{-1}. The SHB technique was originally developed for testing materials under dynamic compressive loading, and is referred to as the Split-Hopkinson pressure bar (SHPB). However, the principles of the SHB have been adapted and the test methods extended to investigate materials under dynamic tension [2–10], torsion [11,12] and shear [13–20]. Whilst a significant number of scientific studies have been issued, building up a sound knowledge database on the dynamic characterisation of materials in compression and tension loading scenarios, only a handful of reliable direct shear setups have been developed, which still limits the understanding of the true dynamic shear behaviour of complex materials.

The present work focuses on the direct assessment of the dynamic shear behaviour of a special class of Fibre-Reinforced Cementitious Composites (FRCCs) that exhibit strain hardening after cracking under

* Corresponding author.
E-mail address: cesare.signorini@tu-dresden.de (C. Signorini).

https://doi.org/10.1016/j.cemconcomp.2025.106212
Received 15 April 2025; Received in revised form 20 June 2025; Accepted 30 June 2025
Available online 1 July 2025

conventional tensile loading, and are known by the acronym SHCCs (Strain-Hardening Cementitious Composites). The investigation is conducted using and critically comparing different SHB shear configurations, which rely on significantly different test principles. SHCCs [21] are promising engineered composites for application in RC members strengthening, characterised by their exceptional mechanical performance and serviceability. Due to the extremely complex interaction of a number of intertwined micromechanical parameters, SHCCs are able to exhibit strain capacities of up to 5 % under tensile loading [22], leveraging the formation of patterns of multiple steady-state opening microcracks. While the dynamic tensile performance of SHCCs has been already extensively investigated [23–28], disclosing high energy absorption capabilities due to their high strain capacity and excellent crack control properties, their shear performance at the material level has not yet been exhaustively addressed by the scientific community through direct testing methods. This aspect is of paramount importance, as research on structural elements subjected to localised impact has widely demonstrated the pronounced punching-shear loading that characterises the impacted zone of a structural element retrofitted with an SHCC protective over-layer [29,30]. However, given the complex nature of shear, inducing a pure shear fracture surface in a dynamic context is not trivial, and the fine tuning of the shear loading configuration, boundary conditions and geometric features of the shear specimen requires careful investigation. Only a few dynamic shear test protocols have been developed and presented for this purpose, mostly utilising the SHB technique. Notable among these is the early introduction of shear testing into a SHB by Hauser [3], using a special prismatic punch-through shear (PTS) specimen placed directly between the input and transmitter bars. Similarly, Xu et al. [15] designed a special PTS specimen inserted directly between the elastic bars of a SHPB, with its transverse motion limited by a special fixture. Lukić and Forquin [16] extended the PTS concept by testing a cylindrical specimen in a SHPB, fixing it between an input rod and a transmitter tube. Building on this idea, Cadoni et al. [19] adopted a similar PTS cylindrical specimen for shear testing in a SHPB, but instead of placing the specimen directly between the elastic rods, a special mechanical connector was developed. Similarly, Guo and Li [14] used a conventional SHPB setup, which was equipped with a specially designed clamping device connected to the transmitter tube to install the PTS sample. In addition to the shear configurations applied on SHB devices, beam-like PTS specimens have been investigated by Ngo and Kim [31] using an impact shear test setup based on a Strain Energy Frame Impact Machine (SEFIM). The comprehensive literature review by Noh et al. [32] identifies only four papers that investigate the dynamic increase factor (DIF) of FRCC by direct testing using a SEFIM at strain rates between 221 and 290 s^{-1}. The DIFs for strength were found to range between 1 and 1.75, although there was a large scatter for peak shear toughness.

A mechanical shear device, recently developed by Tawfik et al. [20], is employed in this work for impact shear testing of SHCC. The shear device is adaptable to two different Split-Hopkinson Tension Bar (SHTB) configurations, i.e. a gravitational version developed by Heravi et al. [10], where the impulse is provided by a free-falling impactor, and a modified version developed by Cadoni et al. [7]. This versatile shear adapter allows the test of double shear specimens (DSS) with a rectangular prismatic geometry, as originally introduced and adopted by Campbell and Ferguson [13]. In addition, the special design of the shear adapter allows high-speed optical measurements followed by Digital Image Correlation (DIC) analysis, and the deformations obtained from DIC can be compared with those calculated from longitudinal wave theory in elastic rods based on mechanical measurements. In addition to the two SHTB setups investigated in this work, a shear configuration based on a SHPB, as described by Cadoni et al. [19], is also considered as a benchmark. The shear SHPB setup involves testing a cylindrical specimen geometry through a PTS configuration using a special coaxial connector between the elastic bars.

The novel contribution of this work lies in the design and execution of a series of direct impact shear tests on an SHCC formulation and its constitutive cement-based matrix using three different SHB configurations. These three test methods follow substantially different principles in terms of load configuration and application, and involve different specimen geometries. The experimental results obtained on statistically robust samples are critically compared with the main objective of defining a way to objectively determine the optimum material properties for the selected SHCC, depending on the test conditions that best reflect the intended application.

2. Materials and methods

2.1. Mixture compositions and experimental program

In this work, two different sample materials are investigated, namely a fine-grained cement-based matrix and a FRCC based on the same matrix. The matrix is based on a blended binder, in which ordinary Portland cement (OPC, CEM I) is partially replaced by fly ash (FA). For this reason, the plain concrete matrix is referred to as “FA” for short. The water/binder ratio of the conglomerate is 0.3, and no coarse aggregates are included in its composition. Instead, fine sand is used to increase the packing density of the fine-grained concrete, thereby improving its strength and preventing excessive shrinkage during setting. Preliminary characterisation of the FA matrix showed compressive and tensile strengths of 60 MPa and 3 MPa respectively after 28 days [24]. The FRCC under investigation is designed starting from the same FA matrix with the addition of ultra-high molecular weight polyethylene (UHMWPE, hereafter PE) fibres in a volume fraction of 2 %. This specific dosage was chosen based on the findings of previous studies [24,33], which demonstrated that the tensile strain capacity of the SHCC could be increased up to 3 %, which is particularly attractive in practice for thin reinforcement layers for damaged concrete structures to improve their impact safety [24,34,35]. The PE fibres, with a length of 6 mm and a diameter of 18 μm, are produced by DSM (The Netherlands) under the brand name Dyneema SK60 [36]. These PE fibres possess a tensile strength of 2500 MPa and a modulus of elasticity of 80 GPa. As common for polyolefin fibres, the PE fibres in use are characterised by a pronounced hydrophobicity, which induces a relatively weak chemical bond with hydraulic matrices [37–39]. However, the intrinsic pull-out rate sensitivity of PE fibres makes them ideal for applications in dynamic load regimes [40]. The two formulations are detailed in Table 1. For FA-FRCC, minor adjustments in the dosages of the binder constituents were deemed necessary compared to FA to adapt the workability of the fresh-state materials.

A total of fifteen experiments were performed on each sample material, i.e. FA and FA-FRCC, with five replicates conducted for each specific SHB configuration. The same mechanical shear device [20,41] was installed in both SHTB configurations, i.e. a gravity-driven [10] SHTB and a modified [7] SHTB. The third configuration, although also designed for shear testing, is based on a SHPB instead. A special coaxial connector, designed specifically for shear testing, is positioned between the elastic bars [19]. A detailed description of all three setups and their

Table 1
Mixture compositions of the FA matrix and FRCC under investigation.

Components (producer)	FA [kg/m^3]	FA-FRCC [kg/m^3]
Cement CEM I 52.5 R-SR3/NA (Holcim, Germany)	519	506
Fly ash (Steag Power Minerals, Germany)	637	620
Quartz sand 0.06–0.2 mm (Strobel Quarzsand, Germany)	536	536
Viscosity modifying agent (SIKA, Switzerland)	2	2
Superplasticizer Glenium ACE 460 (BASF, Germany)	11	11
Tap water	350	341
UHMWPE fibers 2 % by volume (DSM, Netherlands)	–	20

inherent differences is given in Section 2.3, and a summary of the experimental programme is provided in Table 2.

2.2. Specimen preparation

The production of all the shear specimens was divided into three main stages, i.e. (i) mixing and casting, (ii) cutting and (iii) notching. A 3 L batch served to cast a series of specimens for each setup. The mixing phase took place in a Hobart mixer with a volume of 5 L, where the dry constituents were first blended, followed by the incorporation of water and superplasticizer. In the case of FA-FRCC, the short PE fibres were incorporated together with the liquid phases. The detailed mixing procedure is described by the authors in a previous study [20]. The geometry and dimensions of the shear specimens are dictated by the configuration of the shear setup as specified in Section 2.3. Prismatic specimens with a length (L) of 58 mm, a width (W) of 39 mm and a depth (t) of 21 mm were manufactured for both the gravity-driven and modified SHTB. The specimens had top and bottom notches of 7 mm depth lying on the same straight line, resulting in a shear ligament (l) of 7 mm (see Fig. 1a).

For the coaxial SHPB setup, cylindrical specimens were prepared with a depth (t) of 30 mm and a diameter (Φ) of 60 mm. A 20 mm deep concentric notch having a diameter (referred to as inner diameter (φ)) of 30 mm was engraved on the surfaces of the sample to define the shear surface, resulting in a shear ligament length (l) of approximately 10 mm (see Fig. 1b).

2.3. Testing setups

2.3.1. Gravitational Split-Hopkinson Tension Bar

The gravity-driven SHTB was originally developed by Heravi et al. [10] for the specific purpose of testing ductile fibre reinforced cementitious composites under impact tensile loading. This device is installed at the Alfred Hütter Laboratory of the TUD – Dresden University of Technology. The fixture consists of an input bar and a transmitter bar, both made of brass, with a diameter of 24 mm and lengths of 1910 mm and 1900 mm respectively, see Fig. 2a. Brass is preferred to aluminium for this purpose in order to achieve a stress balance within the specimen more rapidly. In addition, previous evidence shows that the relatively low Young's modulus of brass is more effective in reducing noise levels in recorded strain gauge signals [10]. The mechanical shear adapter is integrated between the elastic bars to accommodate the prismatic Double Shear Specimen (DSS), see Fig. 2b, resulting in a shear configuration similar to the Punch-Through Shear (PTS). The specimen is glued to the shear device, using a high-strength bicomponent epoxy resin to prevent its lateral expansion during the test. Fig. 2b shows the installed specimen (21 mm × 58 mm), with its front side positioned in front of the observer (see Fig. 2c for a schematic view). The notches are visible in the narrow space between the upper and lower parts of the shear adapter. With this loading configuration, high shear stresses develop in the two 2 mm shear spans, as can be seen in Fig. 2d, which magnifies the shear-resisting portion of the sample within the adapter.

The strain rate introduced into the experiment is dependent on the drop height of the impactor. The input load tensile wave is generated by dropping a 30 kg steel impactor from any height up to 4 m onto a steel flange connected to the input bar. After impact with the flange, the input bar moves in the direction of gravity. The movement of the lower part of the shear device (lower shear adapter) is rigidly coupled to the movement of the input bar, while the movement of the upper part of the shear device (upper shear adapter) is coupled to the movement of the transmitter bar. In this way, the loading force is generated by the lower adapter, while the reaction force is generated by the upper adapter, as shown in Fig. 2b and c. Two round rubber pulse shapers, 23 mm in diameter and 5 mm thick, are placed on the impacted flange. The purpose of the pulse shapers is to increase the rise time of the wave, resulting in a reduced initial acceleration [42,43], as well as to conform the input waveform to a shape similar to that of the transmitted wave. On the one hand, increasing in the rise time has the significant advantage of drastically reducing inertial effects, thus leading to a more accurate prediction of the actual mechanical properties. On the other hand, it is not possible to attain a constant strain rate in the sample during the test. For the experiments conducted in this work, the drop height of the impactor was 650 mm, resulting in an impact velocity of 3.6 m/s. The resulting input wave is displayed in Fig. 3, with a relatively mild rise time of 900 μs (due to the rubber pulse shapers) and a maximum velocity of 2.3 m/s. Unlike metals, where a distinct plastic zone develops and the nominal strain rate is calculated as an average over the range of plastic deformation, for brittle cementitious materials, the strain rate is usually reported at the point of maximum strength [7].

Strain gauges are used to measure the incident, reflected, and transmitted waves during the impact experiments, with two measuring points on the input bar and one measuring point on the transmitter bar. On the input bar, the strain gauges were glued at a distance of 160 mm and 150 mm from the top and bottom ends of the bar, respectively, while on the transmitter bar, strain gauges were glued at a distance of 160 mm from the lower end of the bar. Force equilibrium, as measured on the input and transmitter bars, was ensured with the impact-shear gravity-driven setup presented, and therefore the one-dimensional wave propagation theory could be applied. The following expressions were applied to calculate the time histories of the shear stress τ, shear slip δ and shear strain rate $\dot{\gamma}$.

$$\tau(t) = \frac{E_0 A_0 \varepsilon_T(t)}{A_s} \tag{1}$$

$$\delta(t) = -2c_0 \int_0^t \varepsilon_R(\zeta) d\zeta \tag{2}$$

$$\dot{\gamma}(t) = \frac{-2c_0 \varepsilon_R(t)}{a} \tag{3}$$

E_0 and A_0 are the elastic modulus and cross-sectional area of the bars, respectively, A_s is the shear cross-sectional area, c_0 is the elastic wave speed in the bar, ε_T and ε_R are the transmitted and reflected strain pulses, respectively, and a is the shear span length.

In addition to the wave analysis from strain gauge measurements, a Photron SA-X2, (480K-M1, Japan) high-speed camera was used to monitor the shear experiment at a resolution of 256 × 376 pixels and a frame rate of 120k fps (frames per second). The optical imaging setup was completed with two Veratis Constellation 120E lights (Integrated Design Tools, USA), which provided continuous lighting at an intensity of 12.5k lm each. Point markers were attached to the adapters of the shear device and their displacements and velocities were monitored using digital image correlation (DIC). Therefore, the shear slip δ_{DIC} and the shear strain rate $\dot{\gamma}_{DIC}$ of the specimen were calculated using the following expressions:

Table 2
Experimental test matrix.

	Description	Gravity-driven SHTB	Modified SHTB	SHPB (PTS – coaxial)
		Number of specimens		
FA	Fine-grained concrete	5	5	5
FA-FRCC	Fibre-reinforced cementitious composite based on the FA matrix	5	5	5

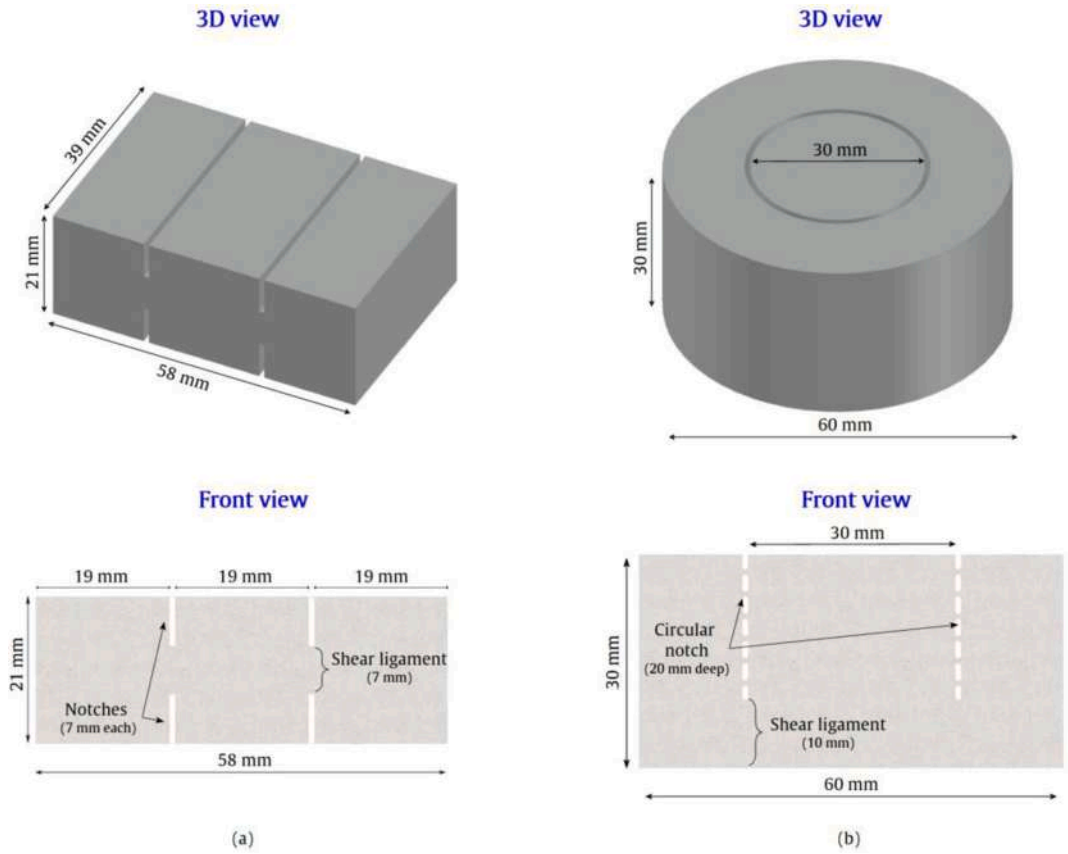

Fig. 1. Geometries and dimensions of the two shear specimens; (a) prismatic and (b) cylindrical.

$$\delta_{DIC}(t) = \delta_{lower}\ (t) - \delta_{upper}\ (t) \tag{4}$$

$$\dot{\gamma}_{DIC}(t) = \frac{v_{lower}(t) - v_{upper}(t)}{a} \tag{5}$$

In Eq. (5), v indicates the velocity of the lower and the upper parts of the shear adapter.

2.3.2. *Modified Split-Hopkinson Tension Bar*

The modified SHTB [7] is used in this work for impact shear testing by incorporating the same mechanical shear device presented in Fig. 2b. The modified SHTB is installed in the DynaMat SUPSI Laboratory of the University of Applied Sciences of Southern Switzerland. The modified SHTB setup along with the integrated mechanical shear device is presented in Fig. 4.

The facility consists of an input and transmitter brass bars, similar to those of the gravity-driven SHTB, each 3000 mm long and 24 mm in diameter. The mechanical shear device is mounted between the brass bars, with its upper and lower adapters connected to the input and transmitter bars, respectively, see Fig. 4b. From their other ends, the transmitter bar is fixed, while the input bar is mechanically connected to a high-strength pre-tensioned steel bar 6000 mm long and 12 mm in diameter. The pre-stressed bar is pulled using a hydraulic actuator at its free end, thus storing elastic energy, while from the other end (connected to the input bar) is connected to a blocking device. The stored elastic energy is released when an intermediate brittle piece fractures due to the applied tensile force, generating a rectangular shaped wave with a duration of 2.4 ms and a rise time of approximately 70 μs. The resulting tensile wave propagates through the input bar, the shear device and transmitter bar. The strain rate of the experiment is finely controlled by the amount of energy stored in the pre-tensioned bar, depending on the stress value applied to prestress it, which must be less than its yield strength. In order to produce an input wave with a similar maximum velocity to that of the gravity-driven SHTB, the pre-tensioned steel bar was loaded with a force of 40 kN. Due to the impedance mismatch between the input brass bar and the pre-tensioned steel bar, only 74 % of the force (29.6 kN) is transferred to the input bar. The resulting input loading wave is presented in Fig. 5 and shows a similar maximum velocity to that produced in the gravitational SHTB, see Fig. 3, but a much shorter rise time (70 μs). This is due to the different methods of inducing the load waves between the two setups, and in particular to the lack of pulse shaping in the modified SHTB, which is intended to simulate a pulse more than 10 times faster than that of the gravitational SHTB. As with the gravitational SHTB, the nominal strain rate is reported at the point of maximum strength.

Two measuring points are used on the input bar to measure the input and reflected waves, with strain gauges are glued at 240 mm from each bar end. Only one measurement point is required on the transmitter bar to record the transmitted wave, where strain gauges are glued at a distance of 240 mm from the end connected to the shear device.

Similar to the gravity-driven SHTB setup, the shear stress τ, shear slip δ and shear strain rate $\dot{\gamma}$ are calculated according to the longitudinal wave propagation theory in elastic rods expressed in Equation (1), Equation (2) and Equation (3), respectively. All experiments were recorded using a Photron Fastcam NOVA S12 (Photron, Japan) high-speed camera with a resolution of 384 × 224 pixels and a frame rate of 100 k fps. A set of three Constellation 120 LED lights with a colour temperature of 5600 K was also mounted to ensure proper illumination of the sample. Again, point markers were glued to the adapters of the shear device to measure their displacements and velocities. Therefore, the shear slip δ_{DIC} and the shear strain rate $\dot{\gamma}_{DIC}$ of the specimen could also be calculated using Equation (4) and Equation (5), respectively. It should be stated that, unlike the gravity-driven setup, the modified SHTB did not exhibit force equilibrium, i.e. the transmitted force is not

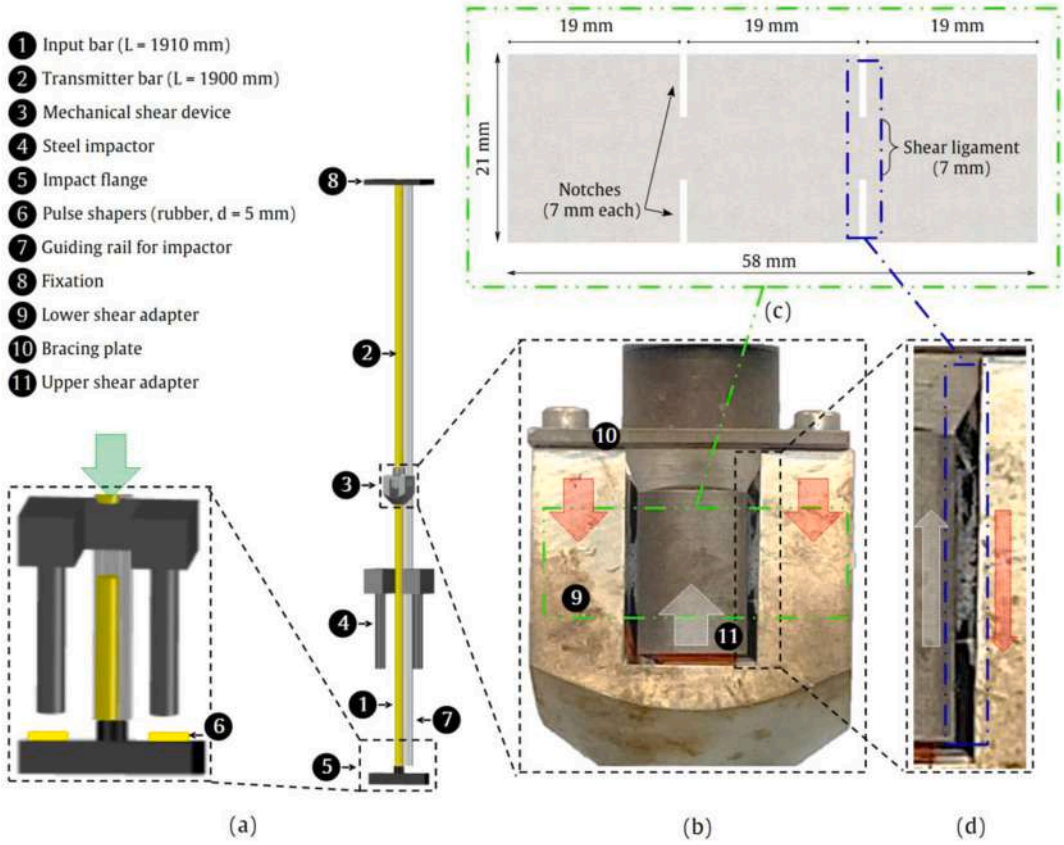

Fig. 2. Gravity-driven Split-Hopkinson tension bar (SHTB) with the integrated mechanical shear device.

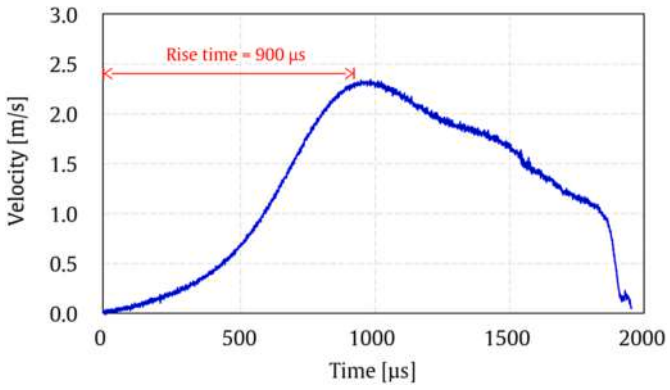

Fig. 3. Input wave produced in the gravity-driven SHTB experiments conducted in this work.

given by the superposition of the input and the reflected forces.

2.3.3. Split-Hopkinson Pressure Bar (SHPB)

The modified SHPB developed by Cadoni et al. [19] is adopted in this work for impact shear testing by incorporating an axial-symmetric mechanical shear device. The modified SHPB is installed in the DynaMat SUPSI Laboratory (see Fig. 6).

The setup consists of input and output aluminium bars, each 3000 mm long and 30 mm in diameter. The mechanical axial-symmetric shear device is placed between the output aluminium bar and the sample. From their other ends, an elastic spring pre-compresses the output bar slightly (20–30 N) to hold the shear device and the sample in place prior to testing, while the input bar is mechanically connected to a high strength steel pre-tensioned bar 6000 mm long and 12 mm in diameter. A hydraulic actuator pulls the pre-tensioned bar at its free end, while the other end, in contact with the input bar, is connected to a blocking device. The stored elastic energy is released when an intermediate joint of brittle material close to the hydraulic actuator breaks, generating a rectangular wave with a duration of 1.2 ms and a rise time of about 300 μs, which propagates through the input bar, the shear device and the transmitter bar. Based on the stress value applied to pre-stress the striker rod, the strain rate level is determined by the amount of energy stored in it. In order to produce an input wave with a similar maximum velocity to that produced by both the gravity-driven and in the modified SHTB, the steel pre-tensioned bar was preloaded at 32 kN. It should be noted that with this preload, no rupture is achieved in FA-FRCC samples and, for this reason, the preloaded was increased to 40 kN.

Due to the impedance mismatch between the aluminium input bar and the pre-tensioned steel striker, only 68 % fraction of the force (27.2 kN) is transferred to the input bar. The resulting input load wave is shown in Fig. 7 and exhibits a slightly higher maximum velocity (2.7 m/s) than that produced by the gravitational and in the modified SHTB setups (2.3 m/s), and a rise time of approximately 300 μs. The experiments were monitored using a single Photron Fastcam NOVA S12, which features a resolution of 512 × 432 pixels and a frame rate of 50k fps. The same set of three Constellation 120 LED lights as mentioned in the previous section were mounted to illuminate the specimen. A lateral high-speed camera (IDT-MotionPro Y4-S3) with a resolution of 416 × 472 pixels and a frame rate of 20k fps was mounted to film the test for the purpose of accurate observation, but not for measurement.

3. Results

3.1. Split-Hopkinson Tension Bars

The time histories of the input and reflected waves for representative

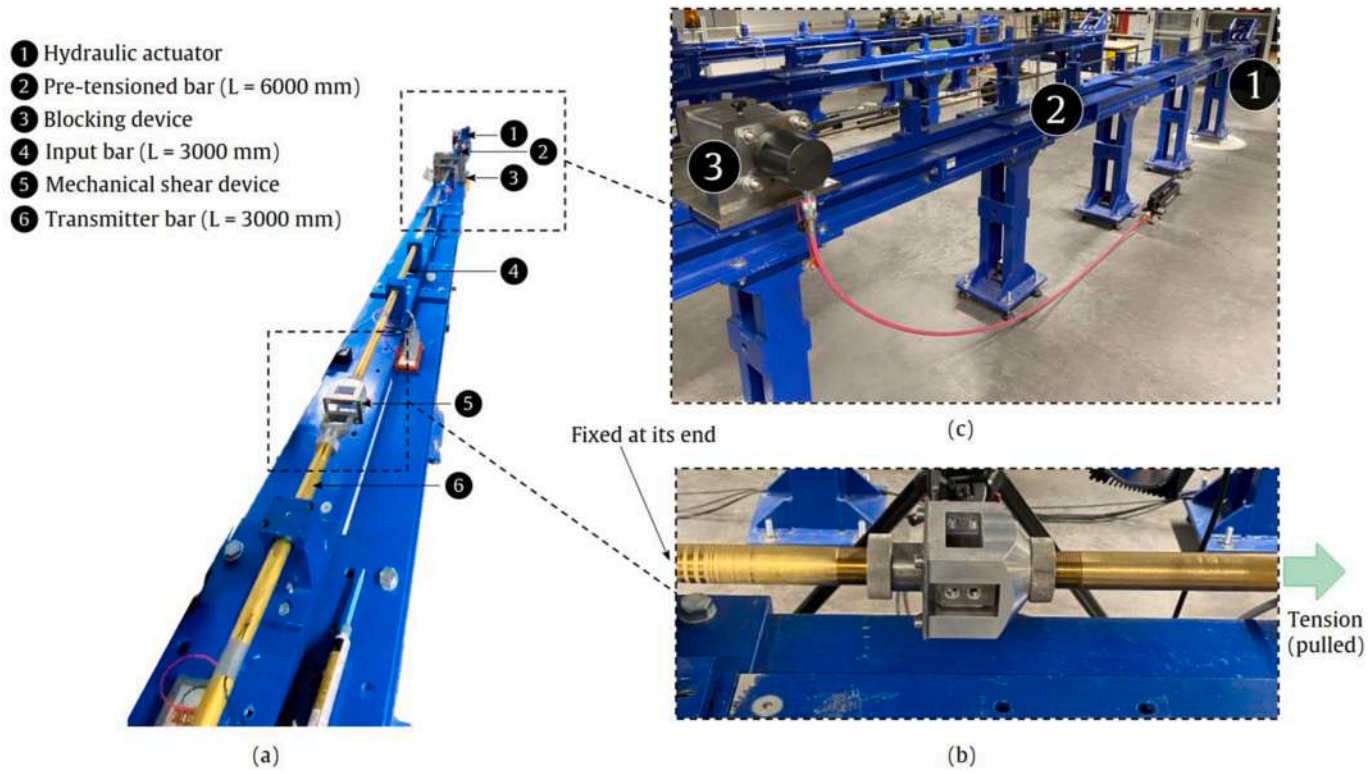

Fig. 4. Modified Split-Hopkinson tension bar (SHTB) with the integrated mechanical shear device (b) along with the setup for load wave generation (c).

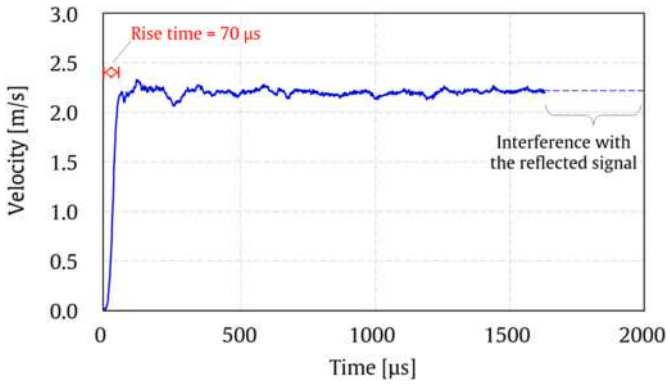

Fig. 5. Input wave produced in the modified SHTB experiments conducted in this work.

specimens of the FA matrix and corresponding FA-FRCC alternatively tested in the gravity-driven and modified SHTB are presented in Fig. 8a and b respectively to mark the differences between the wave profiles generated by each setup. The input waves from the gravity-driven SHTB are characterised by a relatively slow rising branch due to the elastic property of the rubber pulse shapers used between the impactor and the impacted flange.

The ramp-like input wave reduces the strain acceleration and results in a mirrored reflected wave profile in its initial phase, followed by a plateau indicating a constant strain rate. On the other hand, the input waves from the modified SHTB are characterised by the rapid strain acceleration in their initial phase.

The reflected waves in this case initially show rapid scattering, followed by a plateau indicating the constant strain rate achieved. Despite the variation in the input wave generation method of each setup, similar maximum velocities in the input bar were ensured, as can be deduced from the similar slopes of the curves plotting the bar displacements resulting from each input wave profile, shown in Fig. 8c and d for FA matrix and FA-FRCC, respectively.

The shear stress vs. slip and shear strain rate curves for the FA and FA-FRCC specimens tested in the two SHTB setups are presented in Fig. 9, based on the optical measurements and DIC data post-processing. The average apparent shear strengths obtained for the FA and FA-FRCC specimens tested in the gravity-driven SHTB are 34.5 MPa and 35.5 MPa, respectively, while for the modified SHTB they are 35.7 MPa and 38.5 MPa. It is noteworthy that a high extent of agreement was achieved between the shear results obtained from the two testing setups, even though the wave profiles generated were markedly different. As expected, the higher acceleration of the tensile pulse in the modified SHTB compared to the gravitational SHTB resulted in a slight overestimation of the apparent shear strength, on average within 3.5 % for FA and 8.5 % for FA-FRCC. However, this overestimation falls within the usual experimental uncertainty, which is generally much higher for fibre reinforced brittle-matrix composites. Both FRCC and its constituent matrix showed almost similar shear strengths, with no obvious influence of the fibres in the pre-peak phase. However, in the post-peak phase a clear influence of the short PE fibres is observed, which can be explained by the ability of the fibres to transmit residual shear stresses and provide a relatively ductile failure compared to the unreinforced matrix. It can be also seen that there is a very similar overall shear behaviour for each of the materials tested in the gravity-driven setup compared to its counterpart tested in the modified SHTB, with a high degree of consistency.

As another important comparison term, the shear stress vs. slip curves based on shear slip and shear strain rate measured from DIC were compared with those calculated based on the one-dimensional wave propagation theory, as shown in Figs. 10 and 11, for both FA and FA-FRCC, respectively. A representative specimen was selected for comparison. It is clear that there is a certain offset between the slip values calculated using the wave analysis theory and the slip values measured using DIC, due to the non-equilibrium force state present for the modified SHTB setup with such a rapid wave rise, see Figs. 10a and 11a. On

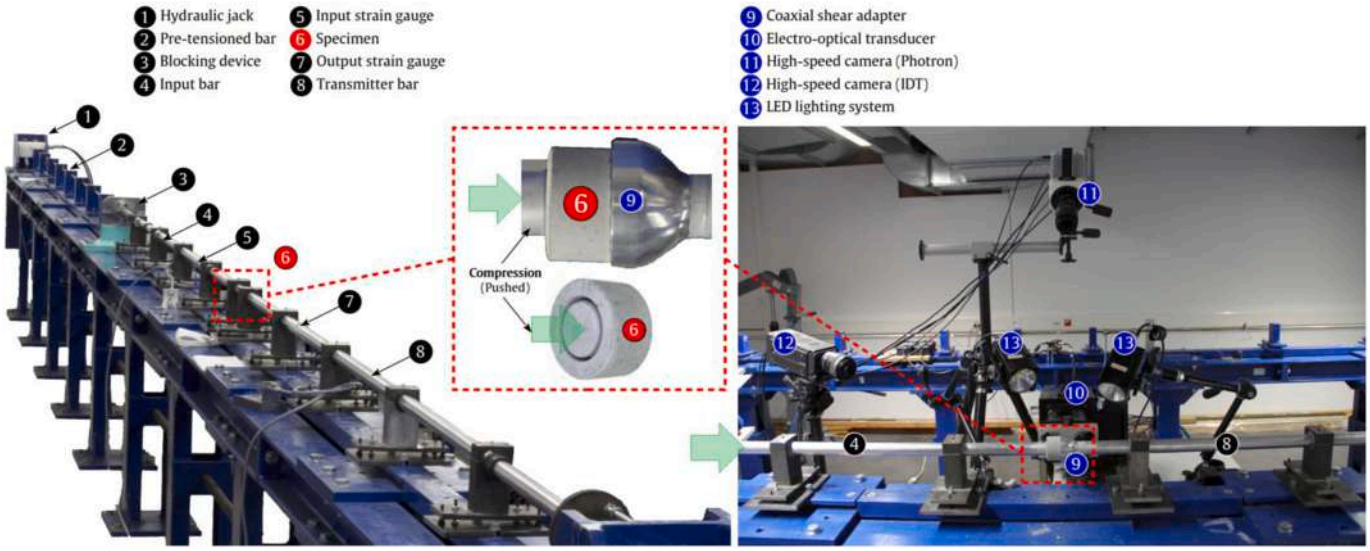

Fig. 6. Modified Split-Hopkinson pressure bar setup (SHPB) with the integrated mechanical shear axial-symmetric device and the measurement setup.

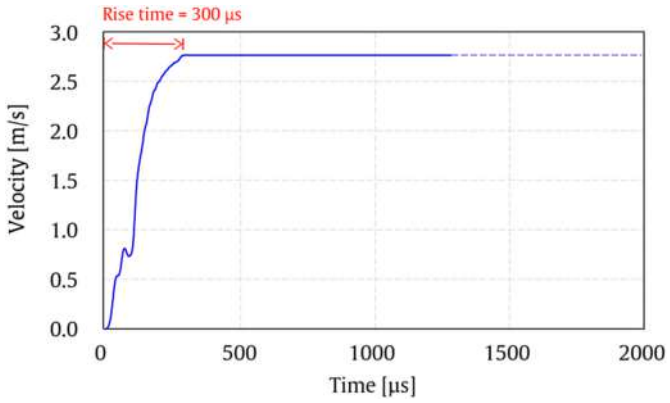

Fig. 7. Input wave produced in the modified SHPB experiments conducted in this work.

the other hand, the DIC measurements and wave analysis calculations from the gravity-driven SHTB experiments are in close match, especially in the pre-peak phase, i.e. before failure initiation, see Figs. 10b and 11b. This is a result of the close proximity of the force equilibrium present in the gravity-driven setup, due to the pulse shaping technique employed.

Frames of an FA-FRCC shear specimen tested in both SHTB setups are shown in Fig. 12, illustrating the progression of shear failure in each case. In both cases, a direct shear-sliding failure is obtained by the formation of a main shear crack in the shear span between the top and bottom notches. As shown by the view of a representative failed FA-FRCC specimen in Fig. 13, the shear failure is tightly localised in the ligament of the notched specimens. Some degree of micro-crack branching in its vicinity is due to the bridging action exerted by the fibres. This action, albeit to a much lesser extent than under tension, contributes to a moderate increase in the toughness of the material when subjected to punching shear at elevated strain rates.

The similarity between the shear failures that occur in both SHTB setups is indeed due to the use of the same mechanical shear device between the elastic bars. As a result, the geometrical characteristics of the specimen are similar and impose an almost similar shear response. This is also reflected in the shear stress vs. shear-slip curves obtained for both test setups for both FA-FRCC and its constituent matrix.

3.2. Coaxial Split-Hopkinson Pressure Bar

Figs. 14 and 15 present the experimental results obtained for 32 kN and 40 kN of preload, respectively. As the FA-FRCC specimens barely reached any failure at the milder preload, the comparisons are outlined on the basis of 40 kN of preload, which produces a wave propagation velocity of approximately 2.8 m/s and a time rise of 300 μs.

Comparing the response of the plain concrete matrix as the loading rate increases, a more brittle response is observed, together with a 15 % increase in the apparent peak load. While showing comparable peak transmitted pulses, the failure for the brittle FA concrete matrix tends to occur in a shorter time frame compared to its fibre-reinforced counterpart, highlighting some increase in ductility provided by the fibres by delaying the crack development to some extent.

Fig. 16 shows the shear stress-slip curves for each specimen tested with the same preload of 40 kN. The SHPB based test setup with coaxial specimen configuration yielded extremely repeatable results characterised by low scatter as demonstrated by the standard deviation bands associated with the apparent shear strength and for the dissipated mechanical fracture energy, calculated as the area under the pulse-slip curve.

Although further investigation would be required to confirm this trend, the inclusion of 2 % by volume of PE fibres in the FA-FRCC formulation resulted in a slight increase in the apparent shear strength. This observation appears to be partially consistent with the findings by Cadoni et al. [19], who found a progressive, albeit more pronounced, increase in shear strength in the case of ultra-high performance concrete with increasing doses of steel fibres, whose aspect ratio (l_f/d_f) was approximately twice that of the PE fibres in this study. Specifically, in the case of 2 % steel fibres, a 44 % increase in strength was achieved [19]. This response obtained with steel fibres could be attributed to their greater length and more effective bridging thereby delaying the crack initiation more effectively. However, a similar decrease in shear slip was found with fibre inclusion in both studies, highlighting strong and complex strain rate interdependencies. Indeed, previous research has demonstrated that in fibre-reinforced concrete, PE fibres tend to switch failure modes from slippage to fibre rupture with moderate DIF in pull-out tests with increasing pull-out rate [23].

This may explain the more brittle response due to premature fibre failure in shear sliding. Fig. 17 shows the failure modes of the coaxial SHPB shear specimens, distinguishing between the brittle FA matrix and its FA-FRCC counterpart.

A dominant shear failure can be clearly seen on the surface of the

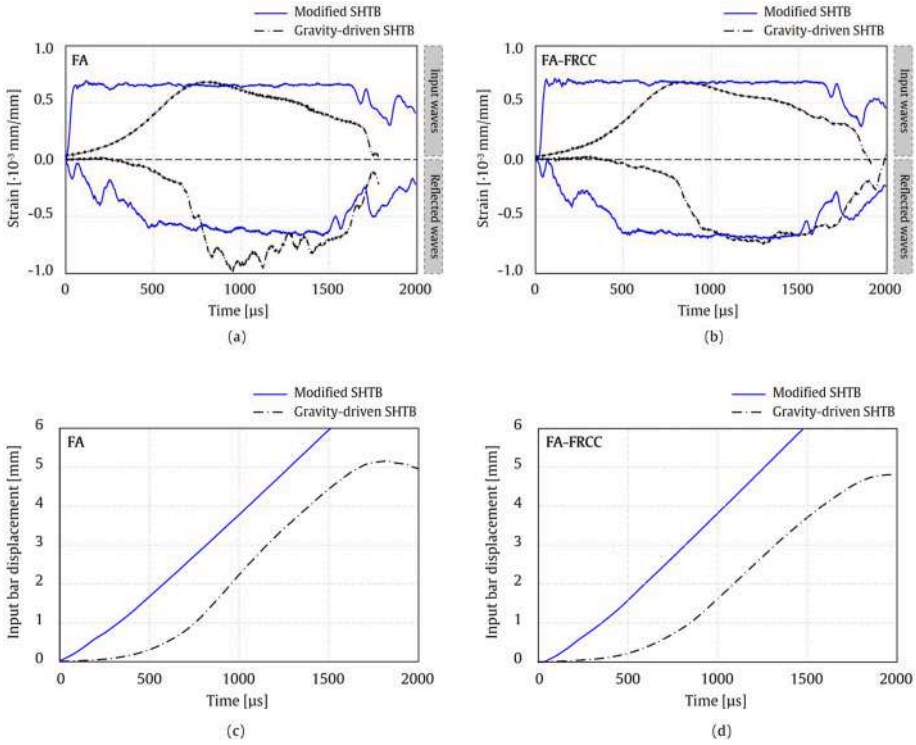

Fig. 8. Input and reflected waves generated in the SHTB setups for (a) FA matrix and (b) FA-FRCC. Input bar displacements based on the input waves SHTB setups for (c) FA matrix and (d) FA-FRCC.

specimens. The brittle failure of the fine-grained concrete matrix is followed by fragmentation of the outer portion of the specimen. On the other hand, the typical failure of the FA-FRCC is characterised by the formation of radial capillary cracks in the outer ring, which are effectively bridged by the fibres anchored in the crack flanks, thus maintaining its integrity. As expected, radial cracks appear in the outer ring of the FA-FRCC specimen after the peak load is attained. The exemplary graph and high-speed camera (lateral) frames in Fig. 18, for one representative FA sample tested with preload of 40 kN, show that radial cracks propagate throughout the specimen way later than the shear failure occurs, thus confirming the reliability of the shear test setup.

4. Discussion

4.1. Failure modes

To better analyse the failure modes of the two sample materials, i.e. FA and FA-FRCC, Fig. 19 shows magnified images of the shear fracture areas of the co-axial shear specimens taken using an optical microscope (Keyence VHX-6000 Video Microscope, Germany) after the test was completed.

A typically brittle behaviour is apparent in plain FA concrete, with the shear fracture area characterised by an uneven surface. The larger matrix flaws in the vicinity of the shear ligament dictate the weakest fracture surface through which the shear crack propagates and slides, and appear directly on the fracture surface. By contrast, the shear fracture zone of FA-FRCC exhibits a neater surface due to the presence of fibres that span and bridge the shear-resistant area. These fibres are pulled out of the concrete matrix and aligned in the same direction as the relative movement of the two parts of the specimen.

In addition, Fig. 20 inspects more closely the behaviour of the PE fibres after the shear test using scanning electron microscopy (SEM, Quanta 250 FEG, FEI, the Netherlands). Extensive and irreversible plastic deformation was observed in the fibres, at both the end of their original embedding channel and in the extracted portion. At the onset of shear sliding, the bridging fibres, which were originally oriented orthogonally to the shear sliding direction as a consequence of the casting process, become kinked in the direction of motion and are extracted from the flank where the embedding length was shorter. Meanwhile, a pronounced deformation is localised in the vicinity of the matrix, where the fibre remains anchored. Fibre plastic deformation, visible throughout the entire pulled-out portion in Fig. 20b contributes to dissipating part of the input energy derived from the impact. Another important factor in dissipation was friction, promoted by the irregular surface of the fibres, characterised by longitudinal grooves resulting from the spinning process of the PE fibres used (see Fig. 6 of Ahmed et al. [44]). During extraction, most of the PE fibres emerging from the crack flank appear to be abraded by friction with the surrounding concrete matrix (see Fig. 20c).

4.2. Effects of boundary and loading conditions

The determination of the mechanical response of cementitious materials and composites is critically dependent on the test conditions, and a general consensus on the best test practices for the specific loading and constraining conditions for accurate characterisation is still needed.

A clear indication of this is provided by the comparative bar chart in Fig. 21, which cross-checks the apparent shear strength of the FA-FRCC and its constituent fine-grained FA concrete matrix when tested in the three different test setups. In all cases, the higher strength of the FA-FRCC compared to the plain FA matrix due to crack formation delay consistently emerged even in substantially different configurations, i.e., SHTB vs. SHPB. The percentage gain in shear load-bearing capacity of FA-FRCC is only marginally different, ranging from 9 % to 13 %, but still reasonably in line with the inherent uncertainties of the material properties themselves. Remarkably, while the two different SHTB setups with the same specimen geometry and load transfer adapter yielded very close results, the coaxial shear tests conducted in a SHPB showed a significantly lower apparent strength values, emphasising the key role played by the specimen geometry, the restraint system and considerable

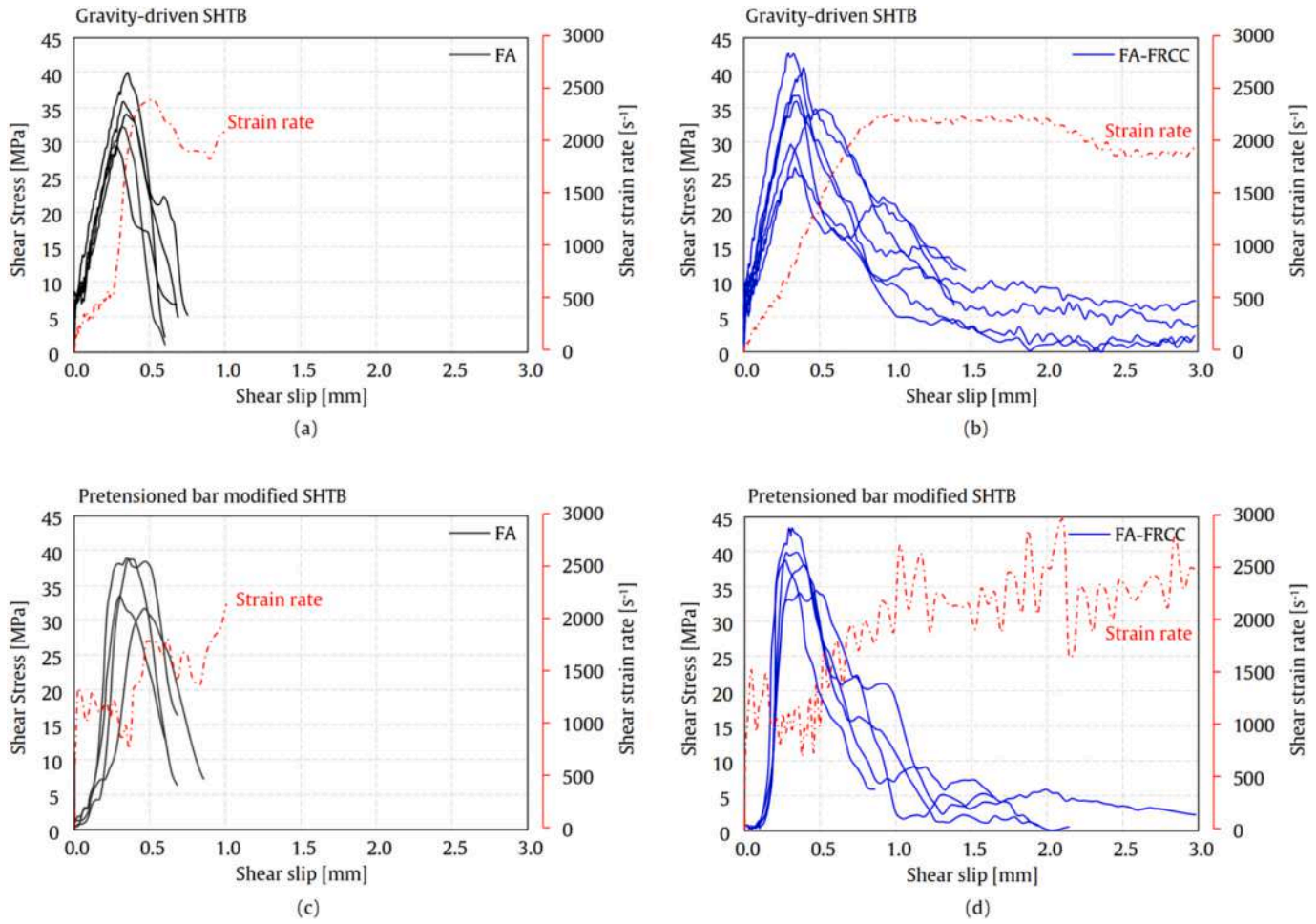

Fig. 9. Shear stress vs. shear strain and shear strain rate for FA and FA-FRCC tested in the two SHTB setups. Deformations are computed from the DIC measurements for a more accurate comparison.

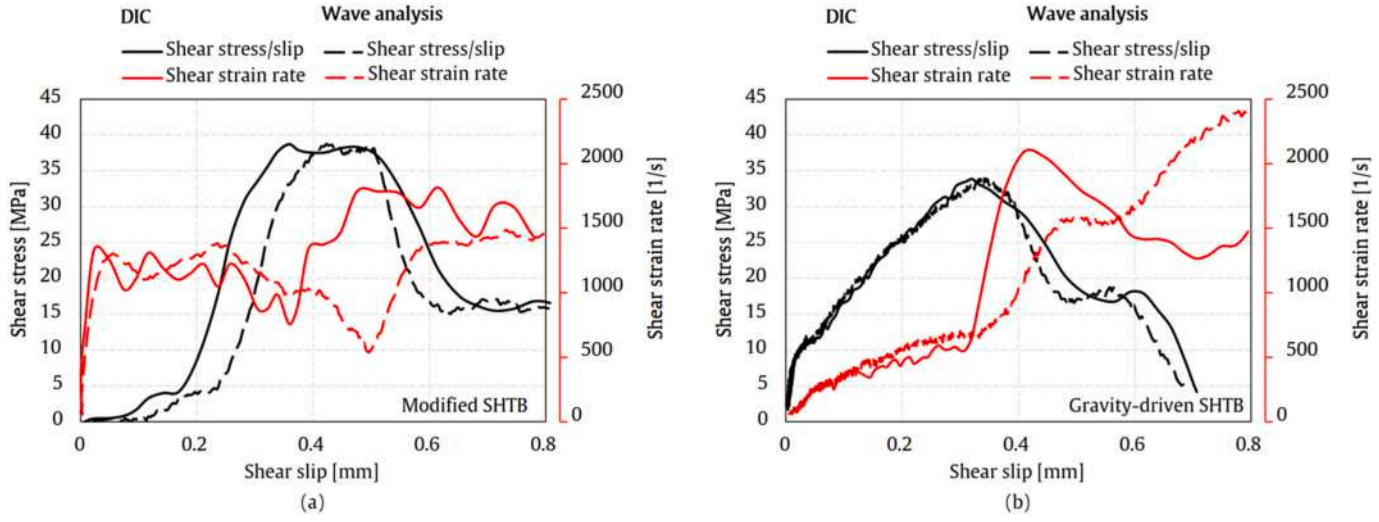

Fig. 10. Comparison between the deformations of a FA matrix specimen measured from DIC and wave analysis as obtained from (a) the modified SHTB and (b) the gravity-driven SHTB.

size effect, which together delineate the extreme sensitivity of the material characterisation. Indeed, it is conceivable that the larger shear resistant area, A_s, of the cylindrical specimen (3.45 times larger, i.e. 943 mm^2 compared to the 273 mm^2 of the DSS specimen) may have increased the likelihood of flaws, which may have reduced the ultimate stress values, the decrease of which is consistent for both types of materials compared to the SHTB results. In addition, the lower apparent strength achieved with the coaxial test in the SHPB could also be

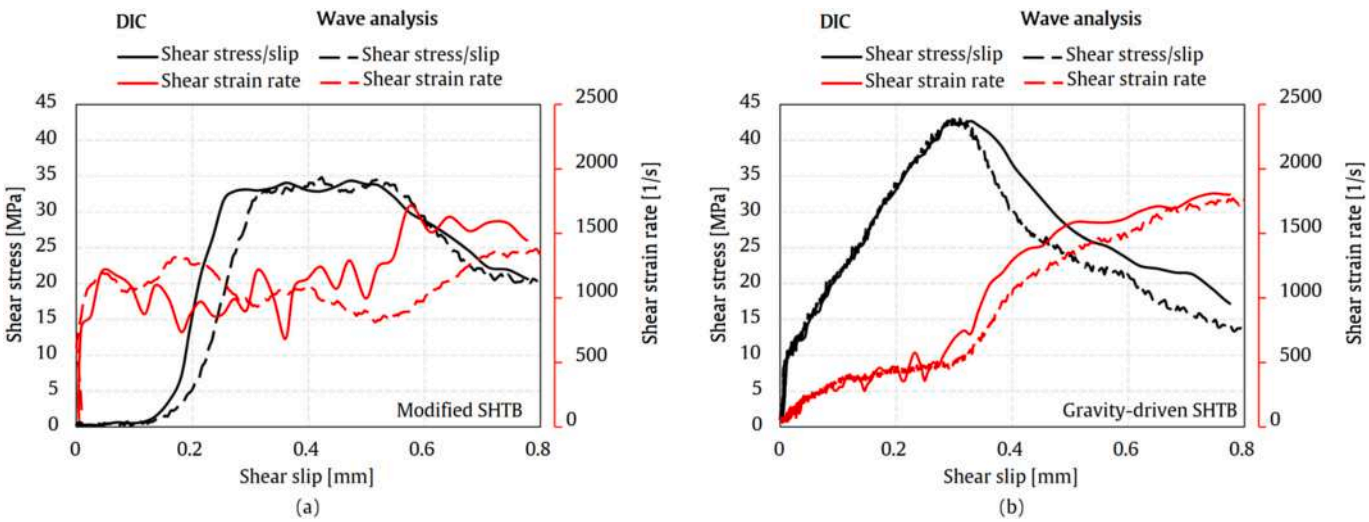

Fig. 11. Comparison between the deformations of a FA-FRCC specimen measured from DIC and wave analysis as obtained from (a) the modified SHTB and (b) the gravity-driven SHTB.

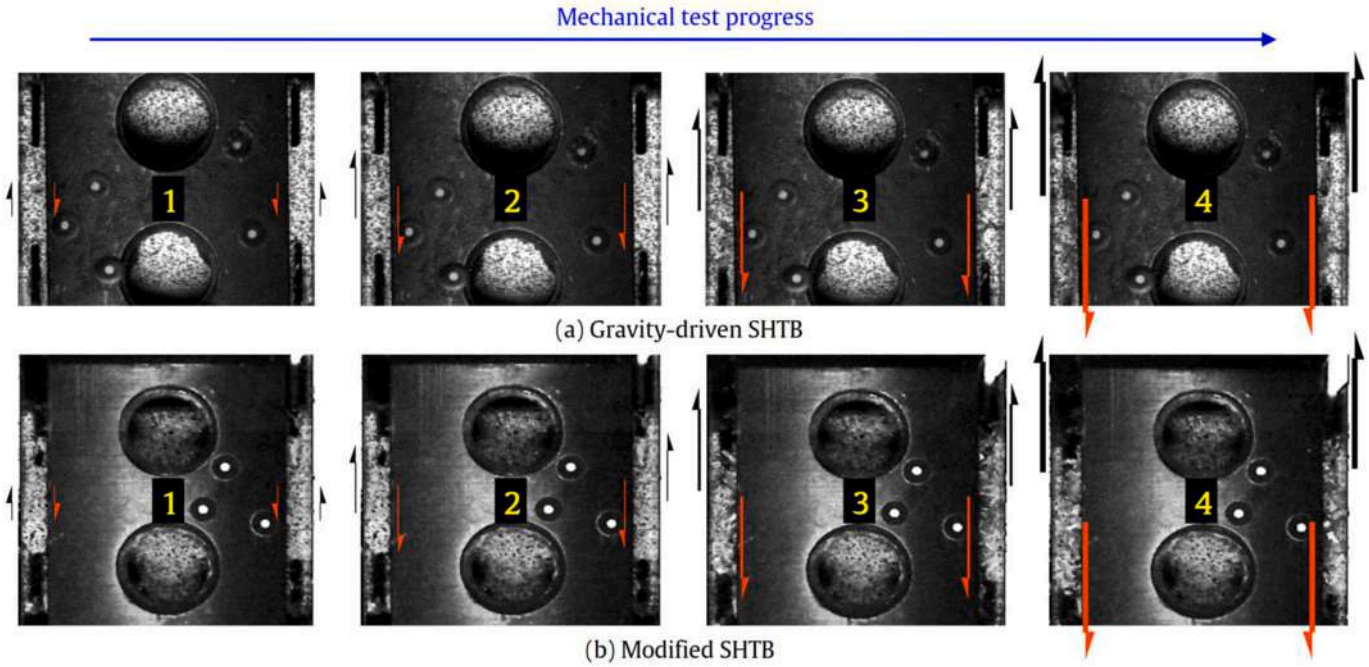

Fig. 12. Frames obtained from the high-speed cameras for a FA-FRCC specimen tested in (a) gravity-driven and (b) modified SHTB setups, illustrating the dynamic experiment and failure progressing.

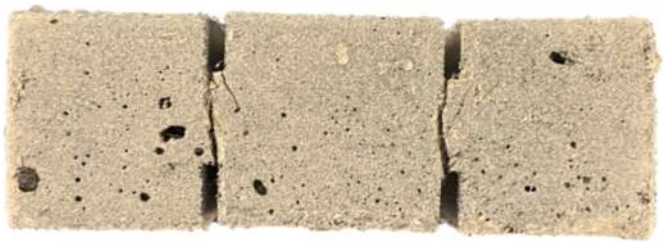

Fig. 13. Failed FA-FRCC sample after test in the modified SHTB.

explained by the looser boundary conditions of the specimen, compared to the other test setups in this work. In the SHTB setups, in fact, the specimen is glued to the support cage of the shear adapter, thereby preventing any degree of freedom of deformation. In the SHPB, there is no confinement for the outer ring of the concentric sample, whose radial cracking is not restricted, as documented by the failure modes observed in Fig. 17. It is then clear that this difference in degree of confinement is the main factor in achieving a different mechanical response of the material. In this regard, Lukić and Forquin [16] have clearly shown the strong correlation between shear and radial stresses and the influence this has in punch-through shear tests, as in the case of our SHPB coaxial test configuration. Contrary to what was suggested there, the absence of an external confinement ring has a strong influence on the test results, as the external concrete ring has the task of resisting the radial distribution of stresses, while the shear span counteracts the shear load.

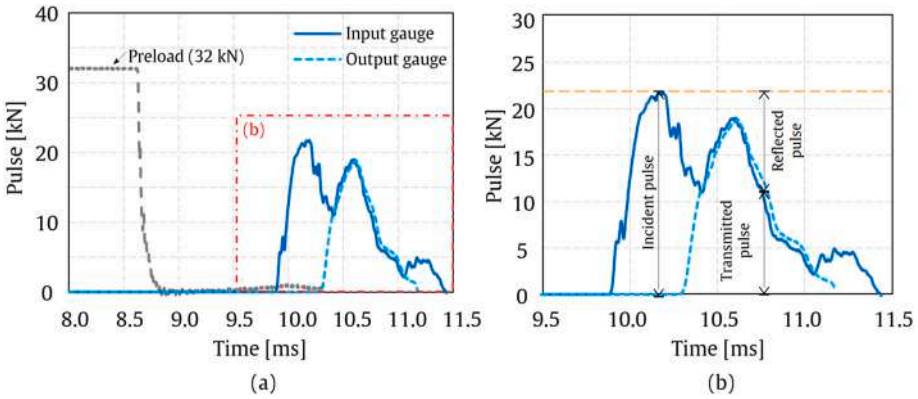

Fig. 14. Test signals for preload, input and output pulses over time for the FA concrete matrix sample with preload at 32 kN.

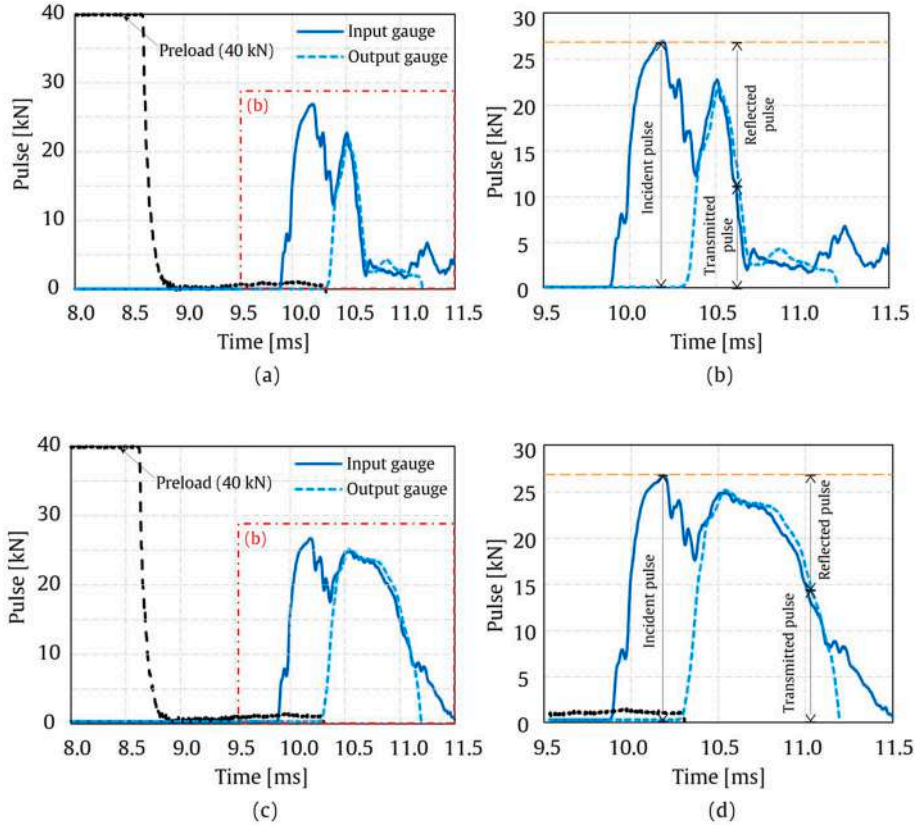

Fig. 15. Test signals for preload, input and output pulses over time for representative FA concrete matrix (a–b) and FA-FRCC samples (c–d) with preload at 40 kN.

5. Summary and conclusions

In this paper, the dynamic mechanical performance of cementitious materials, i.e., a strain-hardening cement-based composite and its plain concrete matrix, has been evaluated by shear testing at elevated shear strain rates. Three different test conditions were investigated in an attempt to characterise the sensitivity of test parameters in the dynamic shear characterisation of cementitious materials, using the most common test approaches, i.e. based on Split Hopkinson Bar. Two of these are based on the same specimen casing device but applied to two different Split-Hopkinson Tension Bars (SHTB), one gravitational and one modified with an external preload system and therefore a completely different shock wave induction in the specimen. The results are critically discussed with those obtained using a completely different shear setup based on a Split-Hopkinson Pressure Bar (SHPB) in a coaxial test configuration. The main conclusions are as follows:

- Material shear properties are highly sensitive to the specimen shape and restraint. The definition of this set of parameters is paramount for obtaining comparable results in SHB shear testing for brittle materials and composites. On the contrary, the wave shape was found to be less critical. In fact, the same specimen dimensions and test mechanisms will give similar results in terms of apparent strength, regardless of the different rise time of the loading wave, provided that the strain rates and wave velocities are comparable.
- The overall material behaviour of brittle-matrix composites is strongly dependent on the boundary conditions of the specimens. Compared to the SHTB configuration where the specimen is glued to the adapter, the results of the PTS-SHPB counterpart with coaxial specimens show that, in the absence of confinement, radial stresses

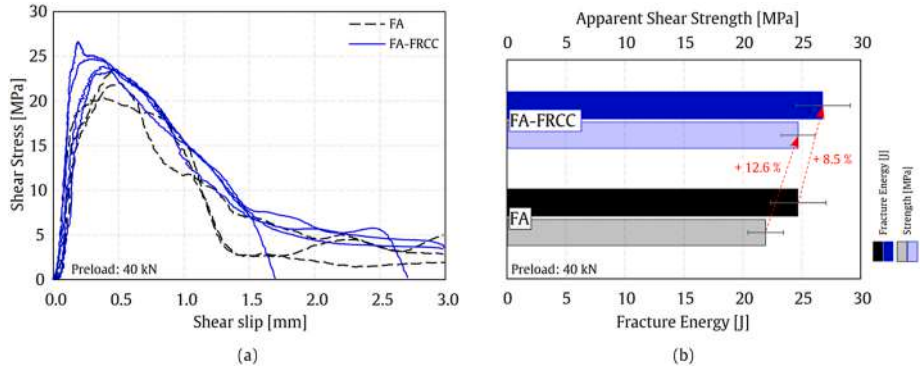

Fig. 16. Shear behaviour of the two materials tested in a coaxial SHPB in terms of shear stress vs shear strain curves (a) and the corresponding performance indices, i.e. apparent shear strength and fracture energy released during shear failure (b).

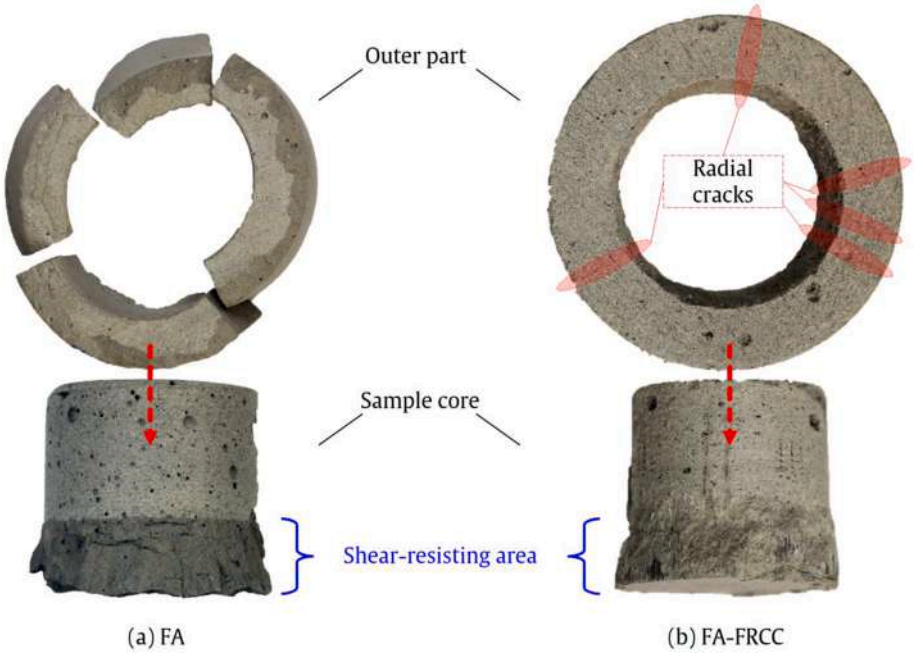

Fig. 17. Representative specimens failed by shear in the co-axial setup of the horizontal SHPB.

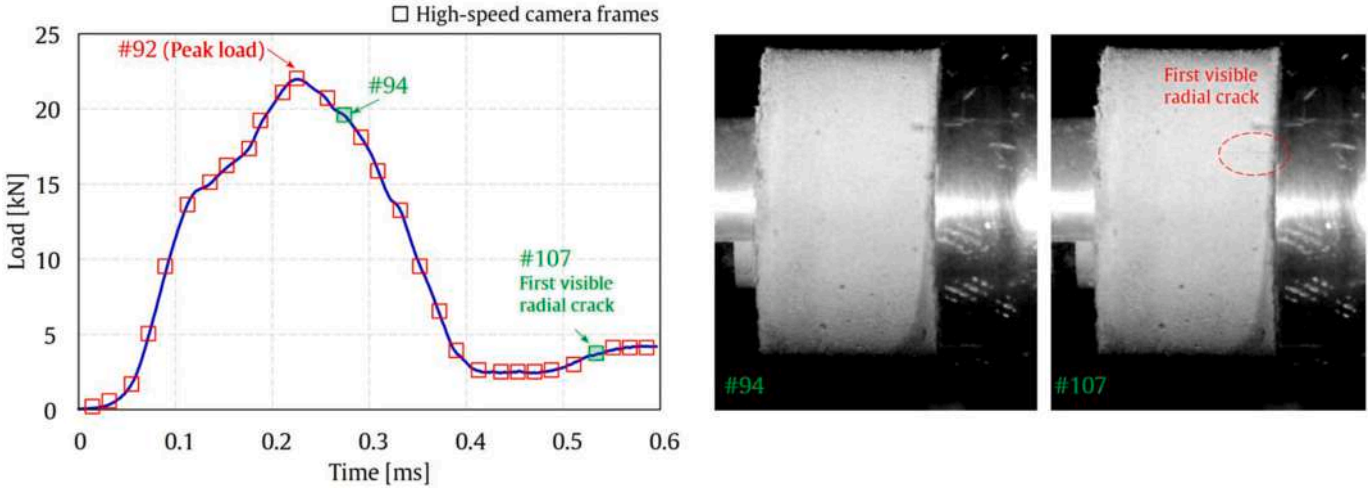

Fig. 18. Load vs time curve for one representative FA sample, along with the corresponding high-speed camera frames. Frames 94 (immediately after peak load and shear failure initiation) and 107 (when the first radial crack passes through the sample) show that shear failure occurs long before tensile failure.

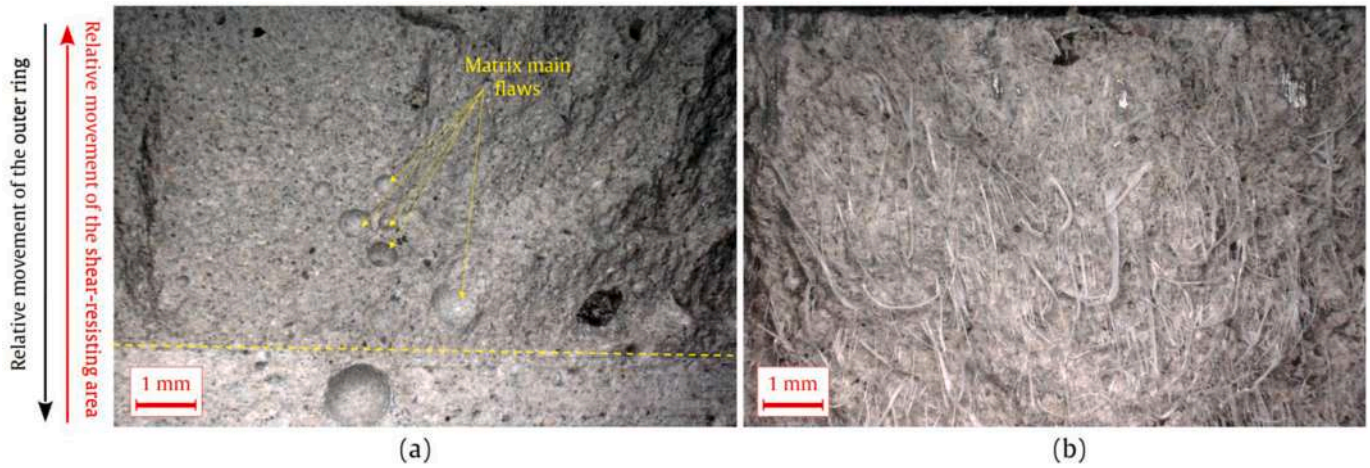

Fig. 19. Appearance of the shear fracture surface of FA (a) and FA-FRCC (b) co-axial shear samples after testing with a preload of 40 kN, as observed using optical microscopy.

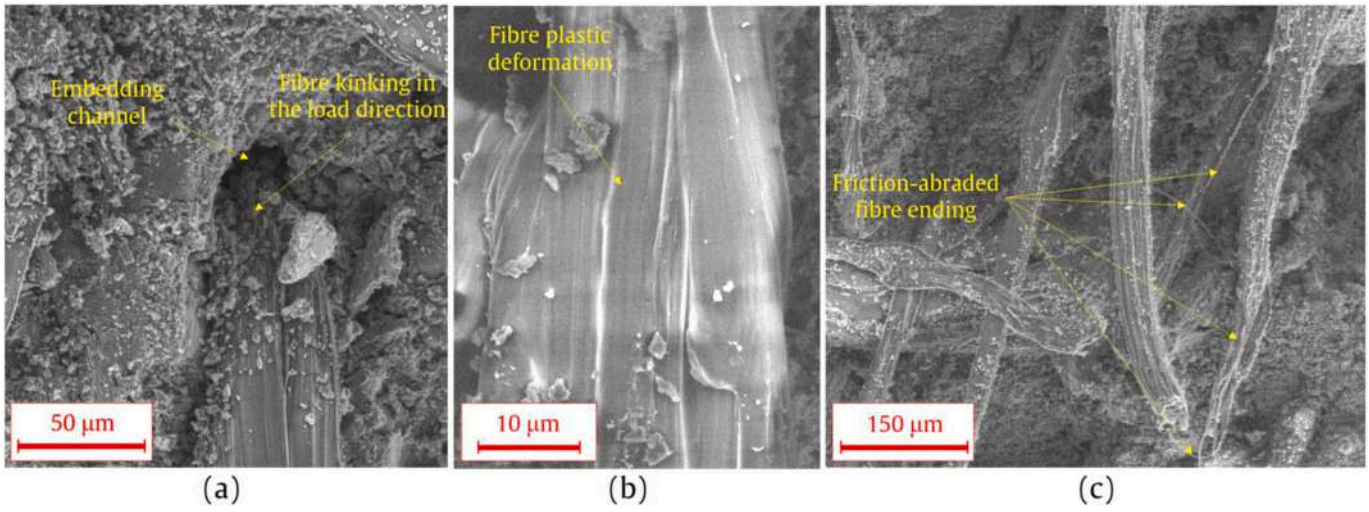

Fig. 20. Scanning Electron Microscopy analysis of the shear fracture surface of a representative FA-FRCC sample, showing the portion of fibre protruding from the matrix (a), a detail of the plastic deformation of PE pulled-out fibre (b) and the fire ending with evident friction-inducted damage.

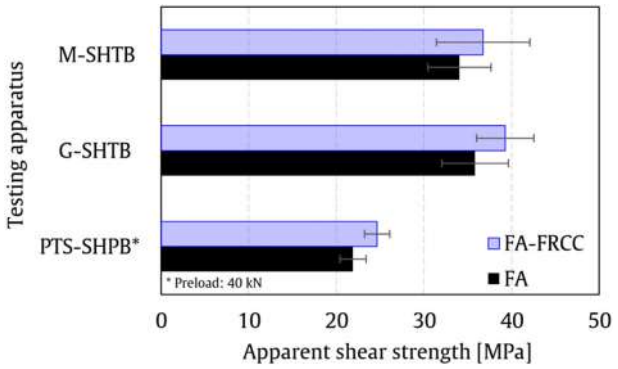

Fig. 21. Apparent shear stress values for the two materials tested depending on the test setup ("M" stands for "*modified*" while "G" stands for "*gravitational*").

are counteracted by the tensile response of the sample material only in the outer ring, thereby resulting in a lower apparent shear strength.

The outcome of this paper highlights the need for standardised test procedures and conditions that could be defined to ascertain the appropriate dynamic material properties according to the specific loading and constraint scenario being sought for specific intended applications.

CRediT authorship contribution statement

Cesare Signorini: Writing – review & editing, Writing – original draft, Visualization, Validation, Supervision, Project administration, Methodology, Formal analysis, Data curation, Conceptualization. **Ahmed Tawfik:** Writing – original draft, Visualization, Methodology, Investigation, Formal analysis, Data curation, Conceptualization. **Daniele Forni:** Writing – review & editing, Validation, Methodology, Investigation, Formal analysis, Data curation, Conceptualization. **Viktor Mechtcherine:** Writing – review & editing, Supervision, Resources, Funding acquisition. **Ezio Cadoni:** Writing – review & editing, Validation, Resources, Project administration, Methodology, Funding acquisition, Formal analysis, Data curation, Conceptualization.

Funding

This work was supported by the German Research Foundation

(Deutsche Forschungsgemeinschaft – DFG) in the framework of the Research Training Group GRK 2250 [grant number 287321140].

Declaration of competing interest

The authors declare that they have no known competing financial interests or personal relationships that could have appeared to influence the work reported in this paper.

Acknowledgement

The authors are grateful to Matteo Dotta (SUPSI) for his precious support in the testing phase. The support of Dr. rer. nat. Thomas Köberle in microscopy analysis is warmly acknowledged.

Data availability

Data will be made available on request.

References

[1] W. Chen, B. Song, Split Hopkinson (Kolsky) Bar: Design, Testing and Applications, Springer, 2011.
[2] J. Harding, L.M. Welsh, A tensile testing technique for fibre-reinforced composites at impact rates of strain, J. Mater. Sci. 18 (1983) 1810–1826, https://doi.org/10.1007/BF00542078.
[3] F.E. Hauser, Techniques for measuring stress-strain relations at high strain rates and typical results presented, J. Soc. Exp. Stress Anal. (1966) 395–402.
[4] M. Li, R. Wang, M.-B. Han, A Kolsky bar: tension, tension-tension, Exp. Mech. 33 (1993) 7–14, https://doi.org/10.1007/BF02322543.
[5] T. Nicholas, Tensile testing of materials at high rates of strain: an experimental technique is developed for testing materials at strain rates up to 103 s−1 in tension using a modification of the split Hopkinson bar or Kolsky apparatus, Exp. Mech. 21 (1981) 177–185, https://doi.org/10.1007/BF02326644.
[6] K. Ogawa, Impact-tension compression test by using a split-Hopkinson bar, Exp. Mech. 24 (1984) 81–86, https://doi.org/10.1007/BF02324987.
[7] E. Cadoni, A. Meda, G.A. Plizzari, Tensile behaviour of FRC under high strain-rate, Mater. Struct. 42 (2009) 1283–1294, https://doi.org/10.1617/s11527-009-9527-6.
[8] G.H. Staab, A. Gilat, A direct-tension split Hopkinson bar for high strain-rate testing, Exp. Mech. 31 (1991) 232–235, https://doi.org/10.1007/BF02326065.
[9] R. Gerlach, C. Kettenbeil, N. Petrinic, A new split Hopkinson tensile bar design, Int. J. Impact Eng. 50 (2012) 63–67, https://doi.org/10.1016/j.ijimpeng.2012.08.004.
[10] A.A. Heravi, I. Curosu, V. Mechtcherine, A gravity-driven split Hopkinson tension bar for investigating quasi-ductile and strain-hardening cement-based composites under tensile impact loading, Cem. Concr. Compos. 105 (2020), https://doi.org/10.1016/J.CEMCONCOMP.2019.103430.
[11] Y. Bai, Q. Xuc, Y. Xu, L. Shen, Characteristics and microstructure in the evolution of shear localization in Ti-6A1-4V alloy, Mech. Mater. 17 (1994) 155–164, https://doi.org/10.1016/0167-6636(94)90056-6.
[12] J. Duffy, J.D. Campbell, R.H. Hawley, On the use of a torsional split hopkinson bar to study rate effects in 1100-0 aluminum, J. Appl. Mech. 38 (1971) 83–91, https://doi.org/10.1115/1.3408771.
[13] J.D. Campbell, W.G. Ferguson, The temperature and strain-rate dependence of the shear strength of mild steel, Philos. Mag. 21 (1970) 63–82, https://doi.org/10.1080/14786437008238397.
[14] Y. Guo, Y. Li, A novel approach to testing the dynamic shear response of Ti-6Al-4V, Acta Mech. Solida Sin. 25 (2012) 299–311, https://doi.org/10.1016/S0894-9166(12)60027-5.
[15] Z. Xu, X. Ding, W. Zhang, F. Huang, A novel method in dynamic shear testing of bulk materials using the traditional SHPB technique, Int. J. Impact Eng. 101 (2017) 90–104, https://doi.org/10.1016/j.ijimpeng.2016.11.012.
[16] B. Lukić, P. Forquin, Experimental characterization of the punch through shear strength of an ultra-high performance concrete, Int. J. Impact Eng. 91 (2016) 34–45, https://doi.org/10.1016/j.ijimpeng.2015.12.009.
[17] P. Forquin, R. Abdul-Rahman, D. Saletti, A novel experimental method to characterise the shear strength of concrete based on pre-stressed samples, Strain 58 (2022) e12407, https://doi.org/10.1111/str.12407.
[18] R. Abdul-Rahman, D. Saletti, P. Forquin, Experimental investigation of the confined behavior of concrete under shear loading at high strain rates, 18th Int. Conf. Exp. Mech. (2018) 496, https://doi.org/10.3390/ICEM18-05408.
[19] E. Cadoni, M. Dotta, D. Forni, G. Riganti, Dynamic response of UHPFRCs in direct-shear tests, Procedia Struct. Integr. 28 (2020) 933–942, https://doi.org/10.1016/j.prostr.2020.11.066.
[20] A. Tawfik, I. Curosu, G. Alsous, V. Mechtcherine, A testing device to investigate the properties of strain-hardening cement-based composites (SHCC) under impact shear loading, Int. J. Impact Eng. 167 (2022) 104280, https://doi.org/10.1016/j.ijimpeng.2022.104280.
[21] V.C. Li, On engineered cementitious composites (ECC): a review of the material and its applications, J. Adv. Concr. Technol. 1 (2003) 215–230, https://doi.org/10.3151/jact.1.215.
[22] V.C. Li, S. Wang, C. Wu, Tensile strain-hardening behavior of polyvinyl alcohol engineered cementitious composite (PVA-ECC), ACI Mater. J. 98 (2001), https://doi.org/10.14359/10851.
[23] I. Curosu, V. Mechtcherine, O. Millon, Effect of fiber properties and matrix composition on the tensile behavior of strain-hardening cement-based composites (SHCCs) subject to impact loading, Cement Concr. Res. 82 (2016) 23–35, https://doi.org/10.1016/j.cemconres.2015.12.008.
[24] I. Curosu, V. Mechtcherine, D. Forni, E. Cadoni, Performance of various strain-hardening cement-based composites (SHCC) subject to uniaxial impact tensile loading, Cement Concr. Res. 102 (2017) 16–28, https://doi.org/10.1016/j.cemconres.2017.08.008.
[25] I. Curosu, M. Liebscher, V. Mechtcherine, C. Bellmann, S. Michel, Tensile behavior of high-strength strain-hardening cement-based composites (HS-SHCC) made with high-performance polyethylene, aramid and PBO fibers, Cement Concr. Res. 98 (2017) 71–81, https://doi.org/10.1016/j.cemconres.2017.04.004.
[26] I. Curosu, V. Mechtcherine, D. Forni, S. Hempel, E. Cadoni, On the rate sensitive fracture behavior of strain-hardening cement-based composites (SHCC) depending on fiber type and matrix composition, in: SP-347 Recent Developments of High Strain Rate Mechanics and Impact Behavior Concrete, American Concrete Institute, 2021, https://doi.org/10.14359/51732655.
[27] V. Mechtcherine, O. Millon, M. Butler, K. Thoma, Mechanical behaviour of strain hardening cement-based composites under impact loading, Cem. Concr. Compos. 33 (2011) 1–11, https://doi.org/10.1016/j.cemconcomp.2010.09.018.
[28] V. Mechtcherine, F. De Andrade Silva, M. Butler, D. Zhu, B. Mobasher, S.L. Gao, E. Mder, Behaviour of strain-hardening cement-based composites under high strain rates, J. Adv. Concr. Technol. 9 (2011) 51–62, https://doi.org/10.3151/JACT.9.51.
[29] C. Signorini, F. Bracklow, M. Hering, M. Butler, L. Leicht, T. Schubert, M.A. B. Beigh, B. Beckmann, M. Curbach, V. Mechtcherine, Ballistic limit and damage assessment of hybrid fibre-reinforced cementitious thin composite plates under impact loading, J. Build. Eng. 80 (2023) 108037, https://doi.org/10.1016/j.jobe.2023.108037.
[30] T.C.S.P. Figueiredo, M. Hering, I. Curosu, F. Bracklow, S. Scheerer, M. Curbach, V. Mechtcherine, F.D.A. Silva, Effect of shear reinforcement and external strengthening with strain-hardening cement-based composites (SHCC) on the impact resistance of reinforced concrete beams, Cem. Concr. Compos. 145 (2024) 105371, https://doi.org/10.1016/j.cemconcomp.2023.105371.
[31] T.T. Ngo, D.J. Kim, Shear stress versus strain responses of ultra-high-performance fiber-reinforced concretes at high strain rates, Int. J. Impact Eng. 111 (2018) 187–198, https://doi.org/10.1016/j.ijimpeng.2017.09.010.
[32] H.W. Noh, V.D. Truong, J.Y. Cho, D.J. Kim, Dynamic increase factors for fiber-reinforced cement composites: a review, J. Build. Eng. 56 (2022) 104769, https://doi.org/10.1016/j.jobe.2022.104769.
[33] V.C. Li, From micromechanics to structural engineering -the design of cementitious composites for civil engineering applications, Struct. Eng. Eng. 10 (1993) 37–48.
[34] C. Signorini, A.H. Ahmed, M. Liebscher, J. Zhao, T. Köberle, V. Mechtcherine, Hybrid fibre-reinforced cementitious composites with short polyethylene and continue carbon fibres: influence of roving impregnation on tensile and cracking behaviour, Mater. Des. 248 (2024) 113465, https://doi.org/10.1016/j.matdes.2024.113465.
[35] F. Bracklow, C.M. Jackson, C. Signorini, E. Jacques, B. Beckmann, M. Curbach, V. Mechtcherine, Hybrid mineral-bonded protective layers for enhanced self-centering capacity of reinforced concrete beams subjected to blast, Eng. Struct. 322 (2025) 119151, https://doi.org/10.1016/j.engstruct.2024.119151.
[36] FibrXL Industrial, UHMWPE dyneema fiber - product data sheet (2020). https://fibrxl.com/wp-content/uploads/2020/07/FibrXL-PDS-performance-0720-DEF-Dyneema.pdf.
[37] A. Peled, E. Zaguri, G. Marom, Bonding characteristics of multifilament polymer yarns and cement matrices, Composites Part Appl. Sci. Manuf. 39 (2008) 930–939, https://doi.org/10.1016/j.compositesa.2008.03.012.
[38] A. Peled, H. Guttman, A. Bentur, Treatments of polypropylene fibres to optimize their reinforcing efficiency in cement composites, Cem. Concr. Compos. 14 (1992) 277–285, https://doi.org/10.1016/0958-9465(92)90026-R.
[39] C. Signorini, A. Sola, B. Malchiodi, A. Nobili, Highly dissipative fiber-reinforced concrete for structural screeds, J. Mater. Civ. Eng. 34 (2022) 04022022, https://doi.org/10.1061/(ASCE)MT.1943-5533.0004160.
[40] A.C.C. Trindade, A.A. Heravi, I. Curosu, M. Liebscher, F. De Andrade Silva, V. Mechtcherine, Tensile behavior of strain-hardening geopolymer composites (SHGC) under impact loading, Cem. Concr. Compos. 113 (2020) 103703, https://doi.org/10.1016/j.cemconcomp.2020.103703.
[41] A. Tawfik, C. Signorini, V. Mechtcherine, Direct assessment of the shear behavior of strain-hardening cement-based composites under quasi-static and impact loading: influence of shear span and notch depth, Cem. Concr. Compos. 140 (2023) 105119, https://doi.org/10.1016/j.cemconcomp.2023.105119.
[42] M. Hassan, K. Wille, Experimental impact analysis on ultra-high performance concrete (UHPC) for achieving stress equilibrium (SE) and constant strain rate (CSR) in split Hopkinson pressure bar (SHPB) using pulse shaping technique,

Constr. Build. Mater. 144 (2017) 747–757, https://doi.org/10.1016/j.conbuildmat.2017.03.185.

[43] D.J. Frew, M.J. Forrestal, W. Chen, Pulse shaping techniques for testing elastic-plastic materials with a split Hopkinson pressure bar, Exp. Mech. 45 (2005) 186–195, https://doi.org/10.1007/BF02428192.

[44] A.H. Ahmed, J. Hübner, D. Junger, C. Signorini, M. Butler, M. Liebscher, C. Scheffler, V. Mechtcherine, Engineering low clinker strain-hardening cementitious composites (SHCC) using polyethylene and cost-effective polypropylene fibers: an experimental scale-linking analysis, Mater. Des. 254 (2025) 114051, https://doi.org/10.1016/j.matdes.2025.114051.